International Journal of Nanomedicine

Dovepress
open access to scientific and medical research

Open Access Full Text Article

ORIGINAL RESEARCH

Encapsulation of a nanoporous simvastatin-chitosan composite to enhance osteointegration of hydroxyapatite-coated polyethylene terephthalate ligaments

This article was published in the following Dove Press journal:
International Journal of Nanomedicine

Xiaoquan Ding
Siheng Wang
Wenhe Jin
Xingwang Liu
Jun Chen
Shiyi Chen

Center of Sports Medicine, Department of Sports Medicine, Huashan Hospital, Fudan University, Shanghai 200040, People's Republic of China

Purpose: This study was designed to evaluate the in vitro and in vivo biocompatibility and osteointegration of plasma-sprayed hydroxyapatite (HA)-coated polyethylene terephthalate (PET) ligaments encapsulated with a simvastatin (SV)-chitosan (CS) composite.

Methods: This study compared the in vitro and in vivo bone responses to three different PET ligaments: SV/CS/PET-HA, CS/PET-HA and PET-HA. A field emission scanning electron microscope was used to characterize the morphology, and the in vitro SV release profile was analyzed. MC3T3 cells were cocultured with SV/CS/PET-HA, CS/PET-HA and PET-HA to test their biocompatibility using CCK-8 tests. Osteogenic differentiation was investigated by the expression of marker genes using qPCR. Osteointegration was performed by implanting the PET ligaments into the proximal tibia bone tunnels of male Sprague-Dawley rats for 3 weeks and 6 weeks. The bone-implant interface was evaluated by micro-computed tomography (micro-CT) and histological analysis.

Results: The characteristic nanoporous structures mainly formed on the surface of the plasma-sprayed HA particles in the SV/CS/PET-HA and CS/PET-HA groups. The SV release test showed that the sustained release of simvastatin lasted for 25 days in the SV/CS/PET-HA group. The in vitro studies demonstrated that the SV/CS/PET-HA ligaments induced osteogenic differentiation in the MC3T3 cells, with higher mRNA expression levels of collagen-1, bone morphogenetic protein-2, osteocalcin and alkaline phosphatase than those in the CS/PET-HA and PET-HA ligament groups. The in vivo tests showed that both micro-CT analysis (bone mineral density and bone volume per total volume) and histological analysis (bone implant contact and interface area) revealed significantly higher peri-implant bone formation and less interface area in the SV/CS/PET-HA group than in the other groups.

Conclusion: The SV-CS composite nanoporous structure was associated with the improved biocompatibility and osteogenic differentiation in vitro and enhanced osteointegration process in vivo of plasma-sprayed HA-coated PET ligaments.

Keywords: simvastatin, chitosan, hydroxyapatite, osteointegration, polyethylene terephthalate

Correspondence: Jun Chen; Shiyi Chen
Center of Sports Medicine, Department of Sports Medicine, Huashan Hospital, Fudan University, No.12, Middle Urumqi Road, Shanghai 200040, People's Republic of China
Tel +86 215 288 8255
Fax +86 216 249 6020
Email biochenjun@fudan.edu.cn; cshiyi@163.com

Introduction

Anterior cruciate ligament (ACL) lesions are one of the most common and devastating sports-related injuries and are always accompanied by misalignment, meniscal and chondral defects, and degenerative osteoarthritis. The overall annual incidence of ACL tears is 68.6 per 100,000 person-years in the USA, and the

submit your manuscript | www.dovepress.com
DovePress
http://doi.org/10.2147/IJN.S210687

incidence among youngsters is almost three times that.[1] ACL reconstruction (ACLR) is the current clinical standard to provide mechanical stability to the joint and return to sports in a timely manner.[2] However, selecting a suitable graft material for ACLR is still one of the most difficult challenges. Featured by its mechanical strength and durability in vivo, polyethylene terephthalate (PET) has been fabricated into artificial ligaments and gained widespread acceptance in ACLR. Nevertheless, disadvantages of PET have gradually emerged and drawn increasing attention, such as its difficulty in integrating with the host bone tissue due to its hydrophobicity and chemically inertness, which might compromise its long-term survival as well as its rapid recovery.[3,4]

In recent decades, many explorations (such as surface coating, hydrogels and electrostatic spinning) have been elaborated to enhance the bioactivity and osteogenesis of artificial implants, among which surface coating technology has been supposed to be one of the most efficient method.[5,6] Hydroxyapatite (HA), the main inorganic component of natural bone tissue, has become a typical coating material for bone implants because of its excellent biocompatibility, osteoconductivity and low degradation rate.[7] Since the 1980s, plasma-sprayed HA coating has been considered as a cost-efficient method for metallic implant surface modification. However, the extremely high working temperature of HA (1100°C–1250°C) has impeded the utilization of plasma-sprayed HA on polymers with low melting points. Recently, with the development of low-energy plasma spraying technology, titanium (Ti) or HA was successfully coated on polyether-ether-ketone scaffolds without affecting their composition or crystallinity and showed improvement in biocompatibility and osteogenesis.[8–10] In addition, in our previous study, PET ligaments coated with plasma-sprayed HA showed an increase in cell proliferation, peri-tunnel bone formation and maximum load to failure.[11] Therefore, plasma-sprayed HA coating should be an excellent solution for improving the biocompatibility and osteoconductivity of PET ligaments.

Due to the multifold requirements of artificial implant design for the rapid restoration of anatomical and biomechanical function of orthopedic structures, researchers have suggested that composite materials could enhance both the osteoconductivity and osteoinductivity of artificial implants by combining the advantages of two or more materials, thereby accelerating the in situ bone regeneration process.[7,12] For artificial ligaments, osteointegration is the prerequisite for a rapid recovery after surgery, which means that composite coatings are even more in need. An in vivo study showed that compared to HA-coated Ti, plasma-sprayed MgO and SiO_2 binary-doped HA-coated Ti implants could significantly enhance bone mineralization and could reach the maximum implant pushout force at week 14.[13] Similarly, another study of ultrahigh-molecular-weight polyethylene coated with vascular endothelial growth factor (VEGF)-loaded silk fibroin showed an improvement in the graft-bone healing process in rabbit ACLR models.[14] Therefore, the addition of bioactive molecules could further improve the osteointegration of plasma-sprayed HA coatings.

Simvastatin (SV), a cholesterol-lowering drug, has gained interest as a promising candidate for bone tissue engineering because of its anabolic effect on bone formation and bone mineral density by enhancing osteogenesis and angiogenesis.[15] To date, several studies have suggested that local application of low-dose simvastatin is an efficient way to promote new bone formation and avoid systemic adverse side effects caused by high dosage.[16,17] However, local delivery of simvastatin is affected by the properties of the divert medium, such as polymer composition, hydrophobicity, crystallinity and degradability.[18,19] Chitosan (CS), which is a deacetylated derivative of natural chitin, has drawn much attention in recent years in the tissue engineering field because of its excellent ability to promote wound healing and bone formation, as well as good biocompatibility and biodegradability into nontoxic components.[20] Moreover, as shown in pharmaceutical applications, CS has become a distinctive drug delivery medium due to its capability to bind and enhance the dissolution of poorly soluble drugs.[21] Recently, Soares incorporated 1.0 μmol/L SV into a CS scaffold and found significantly higher calcium-rich matrix deposition on a scaffold/dentin disc assay, suggesting that the SV-CS scaffold is capable of increasing the regenerative potential of dental pulp cells.[22] In addition to being sensitive to the chemical composition of the coating materials, cell adhesion, proliferation, differentiation and detachment strength are sensitive to the surface roughness and increase as the submicron-scale roughness of HA increases, suggesting that further roughening plasma-sprayed HA particles at the submicron scale might enhance the osteogenesis of PET ligaments in vivo.[23,24] In this study, chitosan complemented with simvastatin was used to functionalize PET ligaments coated with plasma-sprayed HA. The objective of this study was to investigate

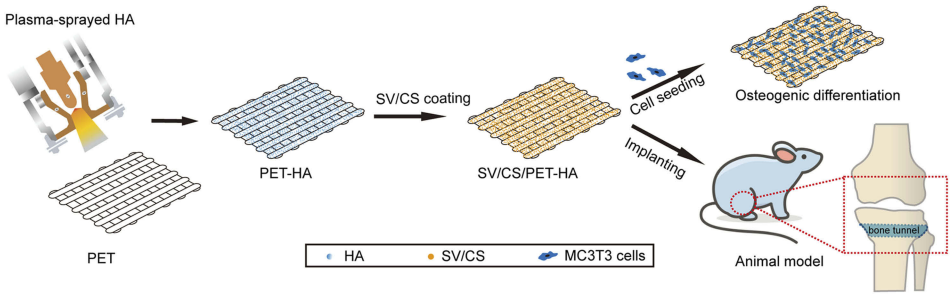

Figure 1 Schematic of the study: the process of preparing the SV/CS/PET-HA ligaments, in vitro osteogenic differentiation and in vivo rat model.
Abbreviations: PET, polyethylene terephthalate; HA, hydroxyapatite; CS, chitosan; SV, simvastatin.

the effect of the SV-CS composite structure on the biological properties of plasma-sprayed HA-coated PET ligaments in vitro and in vivo. As shown in Figure 1, we hypothesized that based on the HA-plasma spraying technology, further encapsulating PET-HA ligaments with the SV-CS composite could promote osteogenic differentiation in vitro and accelerate the bone-implant integration process in vivo.

Materials and methods

Preparation of chitosan/simvastatin functionalized PET-HA sheets

PET sheets were purchased from Ligatech (Shanghai, China). PET sheets were coated with hydroxyapatite (HA) by using the plasma spraying technique according to the previous protocol.[11] 1% (w/v) CS solution (75–85% deacetylated, mole weight 310,000–375,000 d; Sigma-Aldrich, St. Louis, Missouri, USA) in 2% (v/v) aqueous solution of glacial acetic acid was prepared. SV was dissolved in absolute ethanol to 10 mmol/L, followed by drop wise addition to chitosan solution at the final concentration of 10 μmol/L. After rinsed in deionized water 3 times of 30 min and dried at room temperature, HA coated PET was immersed in chitosan solution with or without simvastatin for 1 h at 37 °C, then frozen at −80 °C for 4 h and lyophilized at −20 °C for 24 h to obtain SV/CS enhanced PET-HA sheet (SV/CS/PET-HA) or CS coated PET-HA sheet (CS/PET-HA), respectively. In the following study, three groups were set: SV/CS/PET-HA group, CS/PET-HA group and PET-HA group.

Surface characterization

The morphology of SV/CS/PET-HA, CS/PET-HA, and PET-HA were studied by Field Emission Scanning Electron Microscope (FESEM, Ultra 55, Carl Zeiss AG, Oberkochen, Germany). Image J (version 1.8, National Institutes of Health, Bethesda, Maryland, USA) was used for the HA particle diameter and pore size analysis.

In vitro SV release study

The SV/CS/PET-HA sheets were prepared as 1 cm × 1 cm samples for in vitro drug release study. Five SV/CS/PET-HA samples were immersed in 1 mL sterile Phosphate Buffered Saline (PBS) with constant shaking (120 rpm) at 37 °C. 0.5 mL drug release supernatant was collected and replaced with the same volume of fresh PBS at certain time intervals. The concentration of SV in the release medium was measured by microplate spectrophotometer (Epoch, Bio Tek, Winooski, Vermont, USA) at 240 nm. The cumulative release of SV at various time intervals was quantified according to a standard calibration curve and plotted against time. Samples were measured in triplicate.

In vitro cell test

MC3T3-E1 pre-osteoblast cell line (Cell Bank, Shanghai Institutes for Biological Sciences, Chinese Academy of Sciences, Shanghai, China) was cultured for the in vitro cell test. All the other agents for cell culture were purchased from Thermo (Waltham, Massachusetts, USA), unless noted otherwise. Cells were sub-cultured in flasks using Minimum Essential Medium (αMEM) supplemented with 10% (v/v) fetal bovine serum (FBS) and 100 μg/ml penicillin-streptomycin, maintained at 37 °C in a humidified 5% CO_2 cell culture incubator. Cells were disassociated with 0.25% trypsin-ethylenediaminetetraacetic acid (EDTA), centrifuged and resuspended in completed medium to a cell density of $1x10^6$/mL for further experiments. The PET sheets were cut into 1 cm diameter discs using a commercial punch for the following in vitro cell tests. Before cell seeding, the PET sheets were equilibrated with αMEM containing 10% FBS overnight at 37 °C. In

addition, 500 μL cell suspension was dropped into each well with one sheet at the bottom of 24-well plates, then the PET sheets with cell seeded were transferred into new 24-well plates after 24 h.

For the cell proliferation test, CCK-8 assay was performed at certain time points (the 1st, 4th and 7th days after seeding) according to the manufacture protocol. In brief, 50 μL CCK-8 agent (Dojindo, Kumamoto, Kyushu Island, Japan) was added into each well filled with 450 μL fresh αMEM, and incubate for 2 h at 37 °C. Then 100 μL cell culture medium supernatants were transferred into a 96-well plate and measured at 450 nm using a microplate spectrophotometer.

For in vitro osteogenic differentiation analysis, cell seeded PET sheets were switched to osteogenic media complementing growth media supplemented with 6 mmol/L β-glycerophosphate, 1 nmol/L dexamethasone and 50 μg/ml ascorbic acid. The co-culture samples were further cultured for 4 d and 7 d, changing medium every 2–3 d. The genes: collgen-1 (COL-1), bone morphogenetic protein-2 (BMP-2), osteocalcin (OCN) and alkaline phosphatase (ALP) that marking osteogenic differentiation performance were investigated by quantitative polymerase chain reaction (qPCR) assay. Briefly, total mRNA was extracted by Trizol reagent and converted to cDNA with ReverTra Ace® kits (Toyobo, Kita-ku, Osaka, Japan) according to the manufacture protocols. Sequence of specific reverse and forward primers for target genes and reference gene glyceraldehyde-3-phosphate dehydrogenase (GAPDH) were listed in Table 1. Then qPCR was performed using Thunderbird® SYBR® qPCR Master Mix kits (Toyobo). ABI Prism 7500 qPCR system (Applied Biosystem, Waltham, Massachusetts, USA) was used to amplify the 5 selected genes from each sample in three parallel runs on a 96-well optical reaction plate with the following protocol: 10 min denaturizing at 95 °C, and 40 cycles of 15 s denaturizing at 95 °C, 1 min annealing and extension at 60 °C. The $2^{-\Delta\Delta Ct}$ method was used to evaluate relative fold changes at mRNA expression levels.[25]

Animal surgery

Animal experimental procedures were approved by the Animal Research Committee of Fudan University Animal Science Department, according to the Guide for the Care and Use of Laboratory Animals of National Institutes of Health and the Animal Welfare Act. A total of 30 Sprague-Dawley male rats, 15 weeks old with body weight of 400 ±20 g were used as determined by a power analysis. The rats were divided into 3 groups: SV/CS/PET-HA group (n=10), CS/PET-HA group (n=10), and non-treated PET-HA group (n=10). PET sheets were cut and weaved into PET fiber bundles, 1 mm in diameter and 20 mm in length. Extra-articular traverse bone tunnel model was applied on bilateral proximal tibia. After intraperitoneal anesthesia with 2% (m/v) pentobarbital sodium at the dosage of 1 mL/(100 g body weight), 1 cm anterior midline incision was established, soft tissue surrounding proximal tibia was released from the bone surface and the proximal metaphysis of tibia was fully exposed. The bone tunnel with a diameter of 1.2 mm was drilled from the medial to the lateral along the horizon direction using a Kirschner wire at a slow rotation speed. The remaining bone fragments were washed away by physiological saline. Then a PET fiber bundle was introduced through the bone tunnel using a passing suture. Rinsed the incision with physiological saline repeatedly followed by suturing the muscle and skin carefully. Tibia samples were harvested at the 3rd week and 6th week after surgery for further study.

Micro-computed tomography (micro-CT) evaluation

All the fresh harvested tibia samples were scanned in a SkyScan 1176 micro-CT (Bruker Co. Ltd, Billerica, Massachusetts, USA), using 50 kV and 490 μA with 0.5 mm aluminum filter. Scans were performed using the 18 μm pixel size, 0.5 degrees rotation step, and 180 degrees total scan rotation. Images were reconstructed

Table 1 Primer sequences used for qPCR assay

Gene	Forward primer (5′-3′)	Reverse primer (5′-3′)
COL-1	CCCTGGAAAGAATGGAGATGAT	ACTGAAACCTCTGTGTCCCTTCA
BMP-2	CGGGAACAGATACAGGAA	GCTGTTTGTGTTTGGCTTGA
OCN	CAAGTCCCACACAGCAGCTT	AAAGCCGAGCTGCCAGAGTT
ALP	CCGTGGCAACTCTATCTTTGG	GCCATACAGGATGGCAGTGA
GAPDH	GGCAAATTCAACGGCACAGTC	AAGCAGTTGGTGGTGCAGGA

Abbreviations: COL-1, collegen-1; BMP-2, bone morphogenetic protein-2; OCN, osteocalcin; ALP, alkaline phosphatase; GAPDH, glyceraldehyde-3-phosphate dehydrogenase.

and analyzed by the scanner software NRecon, Data Viewer, CT An and CT Vol (Bruker Co. Ltd.). A column (1.5 mm in diameter and 2 mm in height) within the trabecular region centered on the longitudinal axis of PET implant was defined as the region of interest (ROI-3D), peri-implant bone status, namely bone mineral density (BMD), bone volume per total volume (BV/TV) and bone surface per bone volume (BS/BV) were detected and analyzed.

Histology analysis

Tibia samples reserved for histological analysis were fixed in 4% (w/v) neutral buffered paraformaldehyde solution for 24 h at room temperature following micro-CT imaging, then decalcification with 10% (w/v) neutral buffered EDTA, dehydrated and embedded in paraffin routinely. Tissue sections were 4 μm in thickness, perpendicular to the longitudinal axis of the bone tunnel, and stained with hematoxylin-eosin (HE) and Masson's trichrome, respectively. All the sections were photographed using light microscope (Leica DM6000M, Wetzlar, Germany) with a computer-based image analysis system (Leica LAS V3.8). Similar to that of micro-CT analysis, a 2D circle region of 1.5 mm in diameter that centered on the PET implant was defined as the ROI-2D. The bone-implant interface area (fibrous tissue filled between implants and bone) and bone implant contact (BIC) (the percentage of the bone-implant interface in contact with bone within the total length of the interface) in each ROI were calculated by Image J. At least three noncontinuous sections for each sample were analyzed.

Statistical analysis

All comparisons between the three group were analyzed using One-way ANOVA. $p<0.05$ (*) was regarded as significant, and $p<0.01$ (**) was regarded as highly significant. All assays were conducted with at least triplicate samples. The results were expressed as mean ± standard deviation (SD).

Results and discussion

Microstructural characterization

FESEM was used to characterize the surface morphology of PET sheets in each group. As shown in Figure 2A1–D1, nontreated PET sheets were composed of smooth and homogenically arranged fibers (Figure 2A1–2), while plenty of sphere-shaped plasma-sprayed HA particles were evenly distributed among the PET fibers (Figure 2B1–D1). Interestingly, the FESEM images reveal that the surface of HA particles coated on nontreated PET-HA was smooth (Figure 2B1–2), while the surfaces of HA particles coated on CS/PET-HA (Figure 2C1) and SV/CS/PET-HA (Figure 2D1) were quite rough. The high-magnification images of the CS/PET-HA and SV/CS/PET-HA sheets reveal that the HA particles were characterized by a highly uniformly distributed nanoporous structure (Figure 2C2–D2), indicating that the CS and SV were successfully coated on the HA particles. Figure 2E shows the diameter distribution of the HA particles: ~84.8% of the HA particles were within the diameter range of 10.0–25.0 μm, and the average particle diameter was 17.4±5.9 μm. As shown in Figure 2F, the nanopore sizes ranged from 100 nm to 400 nm (223.9±58.9 nm), of which ~76.9% were concentrated at 150 nm-300 nm.

The reasons underlying the poor osteointegration of nontreated PET ligaments are still uncertain. Much of the literature has attributed these poor outcomes to the hydrophobic and smooth surface.[26] Indeed, several studies have demonstrated that compared to their smooth counterparts, plasma-sprayed HA-coated PET or other polymer materials gain improved hydrophilicity and osteointegration.[10,11,27] Both HA and CS are known as hydrophilic materials, suggesting that the composite coating of HA and CS could synergistically alleviate the hydrophobic properties of PET ligaments. In addition, as shown in the FESEM images, the nanoporous composite structure resulting from SV/CS further enhanced the roughness of the PET ligaments. The published data have shown that submicron-scale texture changes on implant surfaces could provide environmental synergy with respect to osteogenic differentiation and bone formation.[23] In the present study, the combination of hydrophilic materials and nanoscale surface changes could improve the bioactivity of PET ligaments.

Simvastatin release

To locally administer SV and elongate its release process, SV was blended with CS and lyophilized on plasma-sprayed HA particles. According to the previous literature, a low dose (10 μmol/L) of SV was set as the initial coating concentration to avoid the potential cytotoxic effect.[28,29] As shown in Figure 3A, the in vitro release profile of SV from the SV/CS/PET-HA samples in PBS was analyzed by UV-vis spectrophotometry. The data showed an initial burst release (0–70.2%) within the first 5 days. As the incubation time progressed, the SV release rate decreased, and a sustained release of SV lasted for 25 days. These data suggested that low-dose

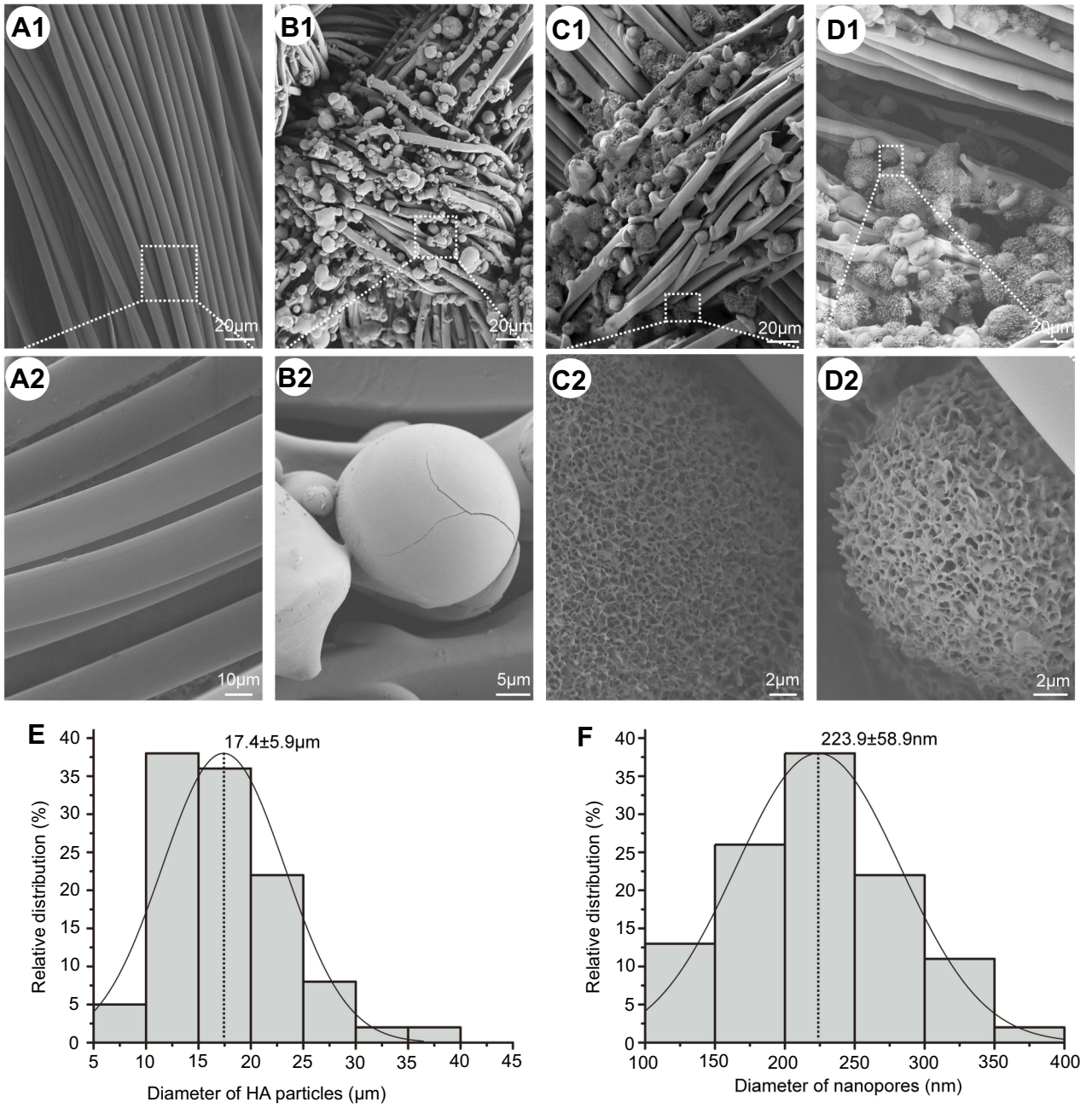

Figure 2 Characterizations of control PET (**A1-2**), nontreated PET-HA (**B1-2**), CS/PET-HA (**C1-2**) and SV/CS/PET-HA (**D1-2**). Diameter distribution of HA nanoparticles in nontreated PET-HA (**E**) and distribution of nanopore size of the SV/CS/PET-HA sheet (**F**).
Abbreviations: CS, chitosan; SV, simvastatin; HA, hydroxyapatite; PET, polyethylene terephthalate; FESEM, Field Emission Scanning Electron Microscope.

SV was loaded on the PET sheets and achieved a sustained release effect.

In vitro cell proliferation and differentiation

According to the CCK-8 data (Figure 3B), SV/CS/PET-HA could promote MC3T3 cell proliferation since the 2nd day. The proliferation levels in all three groups revealed no significant difference on the 1st day, although a higher trend existed in the SV/CS/PET-HA and CS/PET-HA groups. With the elongation of the coculture interval, cells cocultured with SV/CS/PET-HA showed the highest proliferation rate, followed by the other groups ($p<0.01$) on the 2nd, 4th and 7th days. Moreover, the cell proliferation level in the CS/PET-HA group was also higher than that in the PET-HA group on the 4th and 7th days ($p<0.01$), suggesting that SV and CS could synergistically enhance cell proliferation compared with that in the nontreated PET-HA group. In addition to the fact that SV and

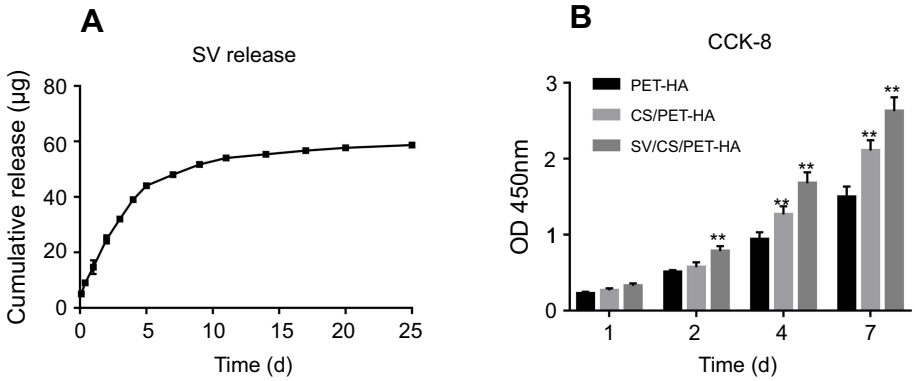

Figure 3 Drug release and CCK-8 assay. (**A**) In vitro cumulative release profile of SV. (**B**) Results of the CCK-8 cell proliferation assay of MC3T3-E1 preosteoblast cells cocultured with PET-HA, CS/PET-HA and SV/CS/PET-HA sheets after 1, 2, 4 and 7 days.
Notes: *p<0.05; **p<0.01, compared with that of PET-HA.
Abbreviations: CS, chitosan; SV, simvastatin; HA, hydroxyapatite; PET, polyethylene terephthalate.

CS have been proven to be bioactive molecules and have been extensively utilized in bone tissue engineering, the roughened surface resulting from the composite coating should also contribute to higher proliferation.[18,30,31]

The expression of osteogenic-specific genes may efficiently reflect the bioactivity or osteoinductivity of the target materials. The expression of osteogenic-related genes, including COL-1, BMP-2, OCN, and ALP, was detected by qPCR in this study at certain time points (the 4th and 7th days). As shown in Figure 4, COL-1, OCN, and ALP expression was significantly upregulated in the SV/CS/PET-HA group compared with that in the PET-HA group on the 4th and 7th days (p<0.01). The BMP-2 expression in the SV/CS/PET-HA group was slightly upregulated on the 7th day compared with that in the PET-HA group (p<0.05) and showed no difference with that in the CS/PET-HA group on the 4th and 7th days. In addition, the trend of upregulated expression of COL-1, BMP-2, OCN and ALP was also found in the CS/PET-HA group compared with that of the control group. However, no significant difference in COL-1, BMP-2 and OCN mRNA expression on the 4th day, as well as that in ALP on the 7th day, was revealed between the SV/CS/PET-HA group and the CS/PET-HA group.

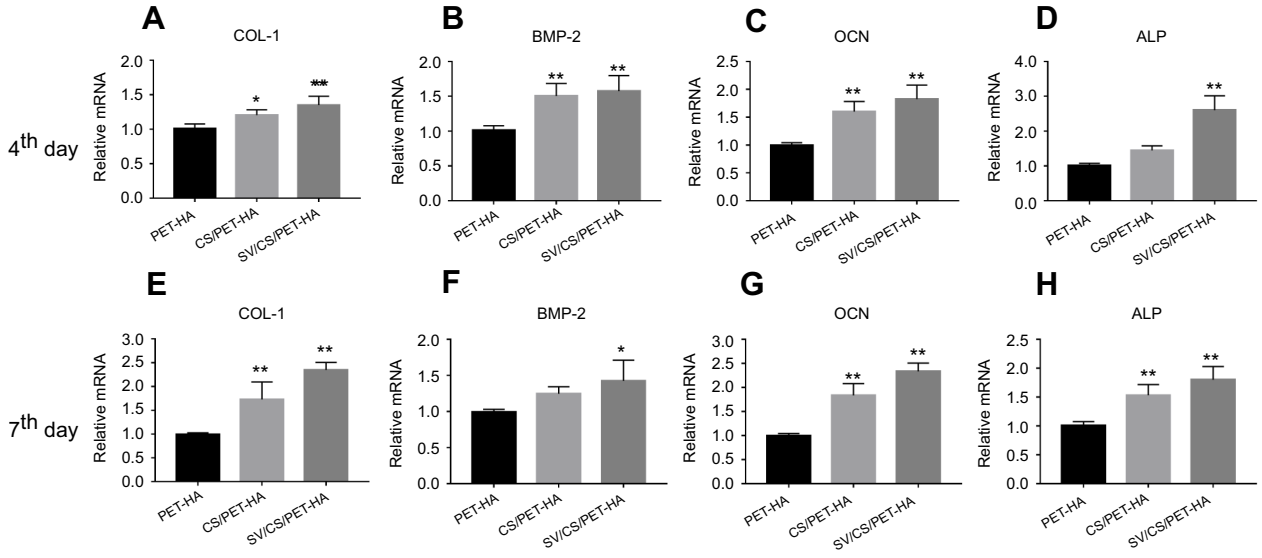

Figure 4 mRNA expression levels of osteogenic-related genes. qPCR analysis was performed for COL-1 (**A, E**), BMP-2 (**B, F**), OCN (**C, G**) and ALP (**D, H**) on the 4th and 7th days.
Notes: *p<0.05; **p<0.01, compared with that of PET-HA.
Abbreviations: CS, chitosan; SV, simvastatin; HA, hydroxyapatite; PET, polyethylene terephthalate; COL-1, collegen-1; BMP-2, bone morphogenetic protein-2; OCN, osteocalcin, ALP, alkaline phosphatase.

Known as the markers of preosteoblast cell maturation and early-phase osteogenic differentiation, COL-1 is the most abundant component of the extracellular matrix, and BMP-2 is an important factor that is involved in initiating and maintaining osteogenesis. ALP and OCN are markers of late-phase osteogenic differentiation and bone mineralization.[32,33] The above data indicated that with the supplementation of osteogenic medium, MC3T3-E1 preosteoblast cells showed a differentiation trend after the 4th day when cocultured with the SV/CS composite. Consistent with the published data, HA, CS and SV could accelerate the osteogenic differentiation process.[18,20,22,34] Once combined, these bioactive materials might show further synergistic effects. However, in favor of its low molecule weight and nanoporous composite structure, SV could be more efficient in the early stage of cell culture, resulting in the short onset time of osteogenic gene expression. Moreover, SV was found to be cytotoxic for osteoblasts at a concentration higher than 10 μmol/L, suggesting that the appropriate dose of SV was a key factor in promoting bone formation.[28] In this study, a concentration of 10 μmol/L was chosen to fabricate the SV-loaded PET/HA sheets. Both the in vitro SV release profile and cell proliferation test demonstrated that the SV level was kept beneath the cytotoxic critical value for MC3T3-E1 preosteoblast cells, and the osteogenic differentiation assay further validated this point. Except for the biochemical stimulatory function of SV and CS, submicron-scale tomography should also be part of the differentiation assay. Several in vitro and in vivo studies have shown that implants with submicron-scale textured surfaces gain greater osteoblast differentiation and bone formation.[24,35] Recently, another study revealed that the submicron-scale surface roughness on 3D scaffolds shows a potential synergistic effect on the ALP activity of osteoblasts in the early stage of culture by inducing the specific adsorption of proteins that influence cell reactions, such as integrin α2β1.[23] In other words, the bioactivity of the SV-CS composite and the nanoporous structure favor cell proliferation and differentiation.

Micro-CT analysis

As shown in Figure 5, to further verify the osteogenesis of the SV/CS-encapsulated PET-HA sheets in vivo, an extra-articular traverse bone tunnel model was established. Micro-CT has been validated for quantitatively analyzing cancellous bone tissue in a preset 3D ROI block around the implants and for evaluating implant osseointegration.[27,36] The reconstructed 3D micro-CT images (Figure 6A1–C2) show that the amount of new bone formed around the implants in the SV/CS/PET-HA group was the greatest, followed by that in the CS/PET-HA group, compared to that in the PET-HA group. Interestingly, the host bone fully enveloped the PET implants and formed sleeve-like structures at the 6th week in the SV/CS/PET-HA and CS/PET-HA groups. As shown in Figure 6D1–F2, quantitative analysis revealed higher BV/TV and BMD values in the SV/CS/PET-HA group (BV/TV: 18.74±3.24, BMD: 0.20 ±0.04) than those of the CS/PET-HA (BV/TV: 13.84±5.37, BMD: 0.15±0.05) and PET-HA (BV/TV: 8.91±3.87, BMD: 0.12±0.04) groups at the 3rd week. At the 6th week, the BV/TV values were 29.74±3.17, 25.03±4.21 and 18.22±5.83 for SV/CS/PET-HA, CS/PET-HA and PET-HA, respectively. Similarly, the BMD values were 0.28±0.05, 0.22±0.03 and 0.16±0.05 for each group in the same order. In addition, the BV/TV and BMD values increased within all three groups compared with those of the 3rd week. However, there was no difference in BS/BV at both the 3rd and 6th weeks. These data suggest that the SV/CS composite nanoporous structure contributes to peri-implant bone formation and mineralization and enhances the osteointegration process.

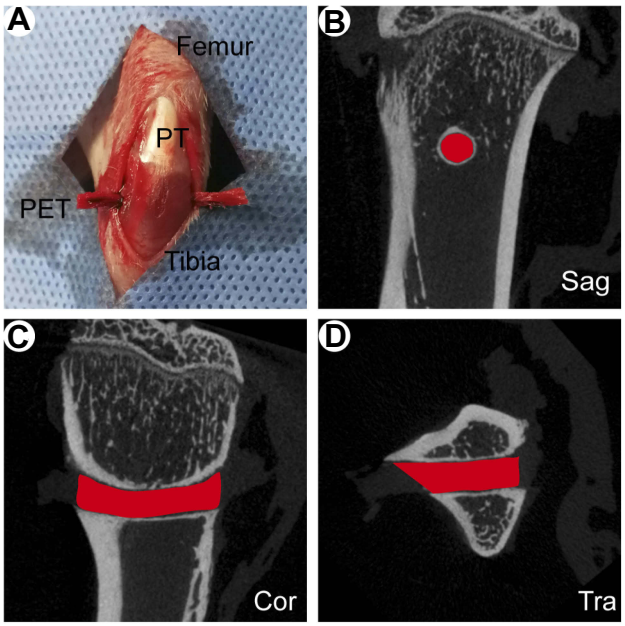

Figure 5 Extra-articular traverse bone tunnel model. (**A**) A PET ligament passing through the tibia bone tunnel. Representative reconstructed 2D micro-CT images of the bone tunnel at the 6th week in the sagittal (**B**), coronal (**C**), and transverse (**D**) planes.
Notes: The red region contoured the PET ligament in bone tunnel.
Abbreviations: PET, polyethylene terephthalate; PT, patellar tendon; Sag, sagittal; Cor, coronal; Tra, transverse.

Histological analysis

To obtain more detailed information on the bone-implant interface, hematoxylin-eosin (HE) and Masson's trichrome staining was performed. As shown in Figure 7A1–2, C1–2,

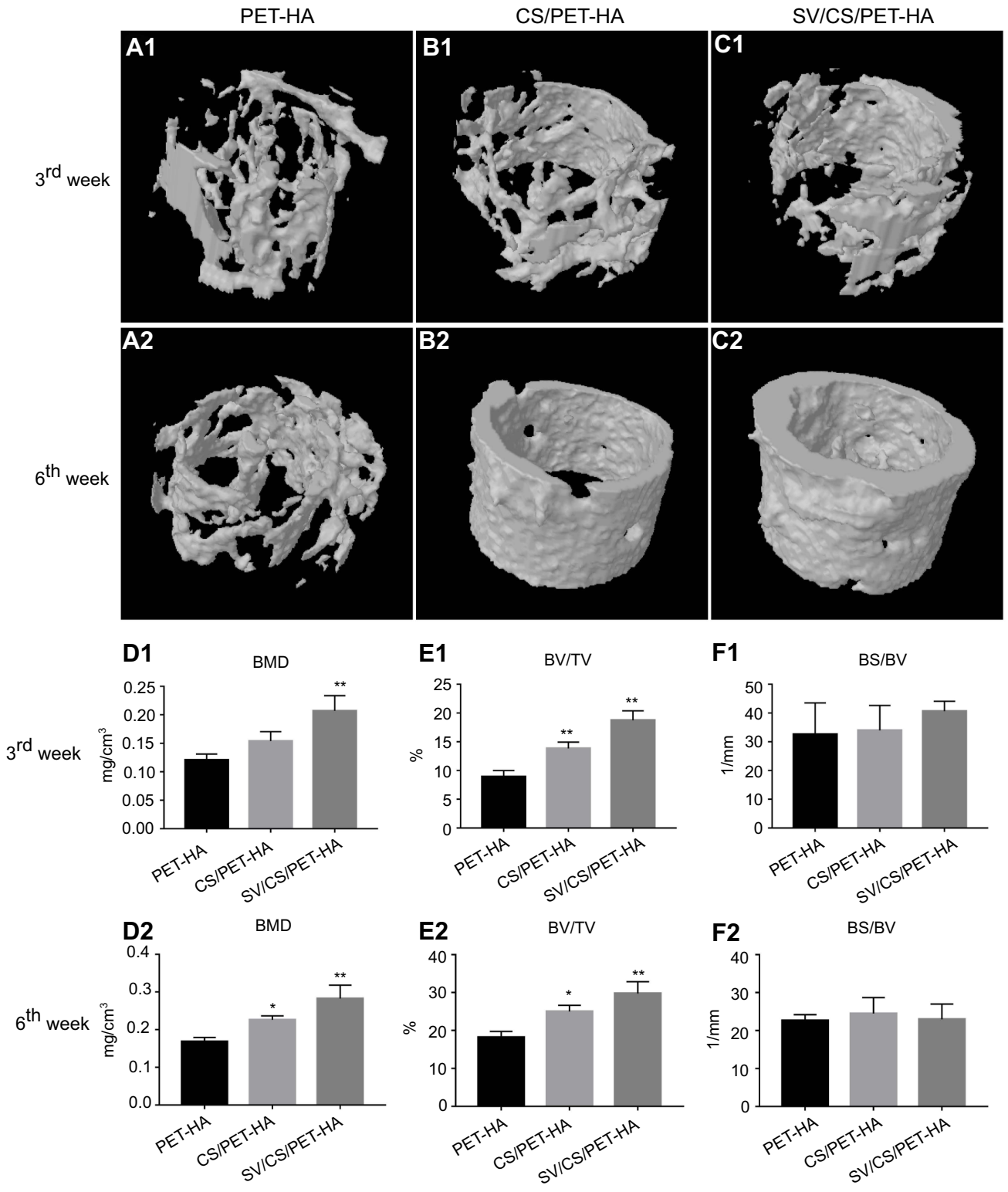

Figure 6 Representative reconstructed 3D micro-CT images of the bone-implant integration at the 3rd (**A1, B1, C1**) and 6th (**A2, B2, C2**) weeks after surgery. Quantitative analysis of the parameters (BMD, BV/TV, and BS/BV) of peri-implant bone at the 3rd (**D1, E1, F1**) and 6th (**D2, E2, F2**) weeks.

Notes: *p<0.05; **p<0.01, compared with that of PET-HA.

Abbreviations: CS, chitosan; SV, simvastatin; HA, hydroxyapatite; PET, polyethylene terephthalate; BMD, bone mineral density; BV/TV, bone volume per total volume; BS/BV, bone surface per bone volume.

E1–2, fibrous tissue formed at the bone-implant interface in all three groups at the 3rd week after surgery; however, much of the fibrous tissue remaining at the bone-implant interface existed only in the PET-HA group at the 6th week. While the new bone formation showed the opposite trend, thin and sparsely distributed cancellous bone was found around the implants in the PET-HA group (Figure 7B1–B2). In contrast, thick lamellar bone enclosed the implant in the SV/CS/PET-HA group (Figure 7F1–F2). In addition, there were less fibrous tissue and more new bone formation in the CS/PET-HA group (Figure 7D1–D2) than in the PET-HA group at the 6th week.

To further quantitatively analyze osteointegration, BIC and interface area evaluation were conducted. As shown in Figure 7G and I, BIC was 23.78±5.24 in the SV/CS/PET-HA group at the 3rd week, higher than that in the CS/PET-HA (17.21±7.38) and PET-HA (11.31±6.51) groups. At the 6th week, BIC increased within each group, and the SV/CS/PET-HA group (54.03±10.18) showed a higher value (p<0.01) than that of the CS/PET-HA (32.46±5.37) and PET-HA (20.31±8.31) groups. In contrast, the interface area (Figure 7H and J) of the SV/CS/PET-HA group was 0.31±0.07 at the 3rd week and 0.17±0.05 at the 6th week, which was significantly lower (p<0.01) than that of the PET-HA group (0.52±0.09 at the 3rd week and 0.39 ±0.07 at the 6th week). Consistent with the micro-CT data, the results of the histological and quantitative analysis suggested that locally released SV promoted the osteointegration process and that CS also contributed to this process.

Using micro-CT and histological analysis, the current study comprehensively evaluated the effects of SV/CS-encapsulated PET-HA ligaments on the osteointegration process in a rat extra-articular model. Although the anterior cruciate ligament reconstruction model likely reflects the clinical situation, one

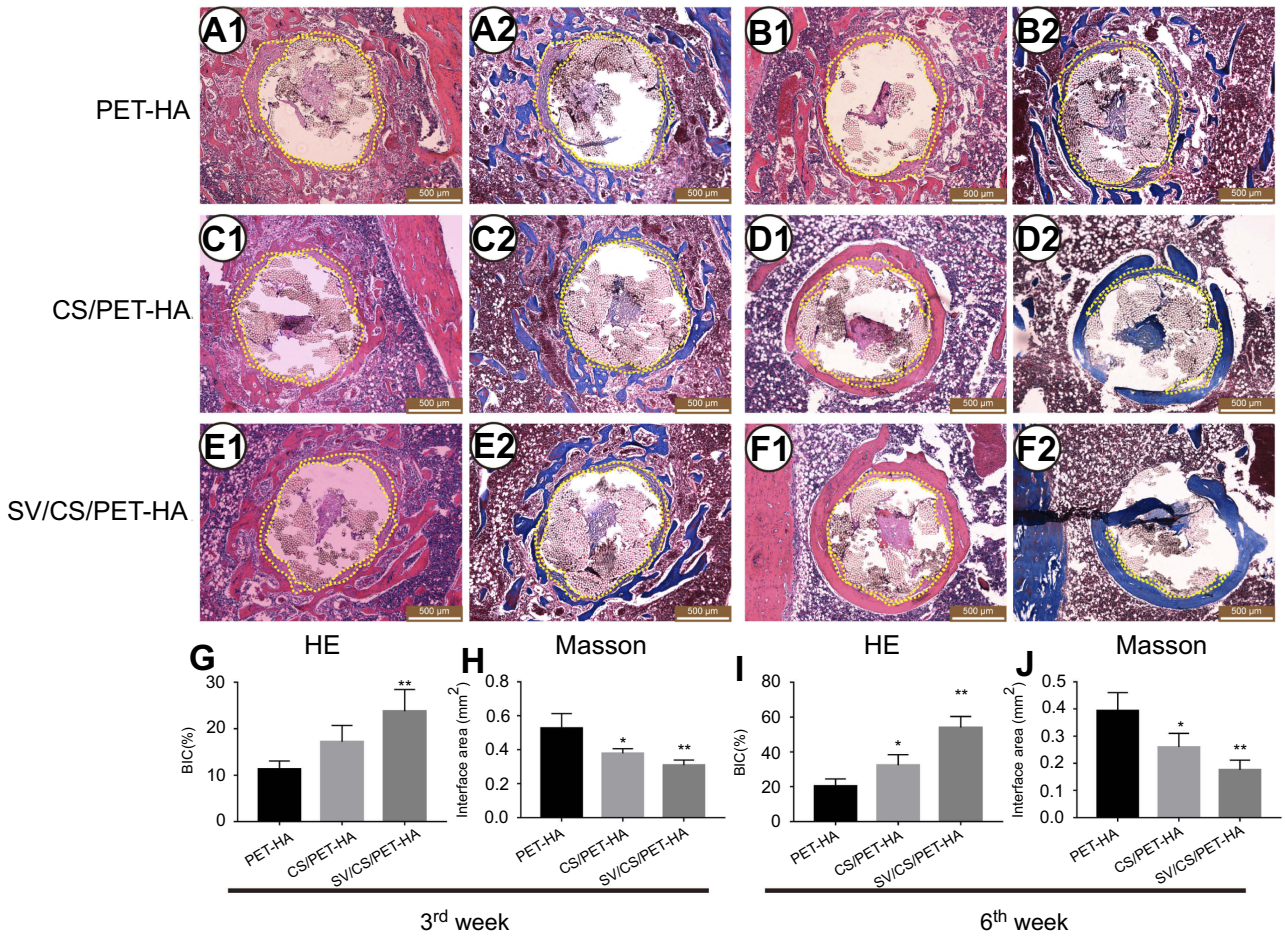

Figure 7 Images of the histological sections and quantitative analysis of the BIC and interface area of bone formation around the implants at the 3rd and 6th weeks after surgery. (**A1, C1, E1**) HE staining and (**A2, C2, E2**) Masson's trichrome staining of corresponding sections showed the bone-implant interface at the 3rd week after surgery. (**B1, D1, F1**) HE staining and (**B2, D2, F2**) Masson's trichrome staining of the corresponding sections showed the bone-implant interface at the 6th week after surgery. Quantitative analysis of the BIC (**G, I**) and interface area (**H, J**).

Notes: The yellow dotted lines contoured the interface area. The original magnification is ×5 for A1-F2, and the bar is 500 μm. *p<0.05; **p<0.01, compared with that of PET-HA.

Abbreviations: CS, chitosan; SV, simvastatin; HA, hydroxyapatite; PET, polyethylene terephthalate; BIC, bone interface contact.

fact should not be neglected: the complex microenvironments within the joint, including the biomechanical factors, as well as the complicated surgical factors, might result in poor reproducibility of the surgery outcome.[37] Consequently, this insufficiency in consistency further magnifies the bias in the accuracy of the outcome. Therefore, this study used a rat extra-articular model to eliminate the influence of complex intra-articular factors and obtained accurate information about bone-implant integration.

Osteointegration is the combination of increased bone ingrowth and reduced fibrous tissue that fill the gap between the bone and implants.[38] Consistent with previous reports, both the in vitro and in vivo results of this study supported that SV facilitates osteogenic differentiation and improves osteointegration.[16,28,39] Furthermore, CS also showed its positive effects on osteointegration in this study. In addition to having excellent biochemical properties, CS has been shown to take part in osteogenesis, angiogenesis and macrophage activation, which could further accelerate new bone growth into an implant surface.[40] According to previous studies, in addition to the chemical composition of the implants, surface topography could also affect cell adhesion, proliferation and differentiation.[23,24] The current study successfully encapsulated PET-HA ligaments with nanoporous SV/CS composites, further increasing the roughness of PET-HA ligaments. The outcomes of the extra-articular bone tunnel model were consistent with those of the in vitro cell tests, showing enhanced peri-implant bone formation and implant bone connection, suggesting that the SV/CS composite and the specific nanoporous structure contribute to the osteointegration process.

Conclusion

In this study, nanoporous HA particles on PET ligaments combined with a simvastatin/chitosan composite were successfully developed, and the loaded simvastatin could be gradually released in a sustainable manner for 25 days. Both the in vitro and in vivo results confirmed that simvastatin-loaded SV/CS/PET-HA ligaments improve biocompatibility and osteogenic differentiation and enhance peri-implant bone formation. This novel SV/CS/PET-HA artificial ligament serves as a promising implant material for ACLR in the future.

Acknowledgments

This work was supported by National Key R&D Program of China (2016YFC1100300, 2017YFC0840100 and 2017YFC0840106), National Natural Science Foundation of China (No. 81572108 and No. 81772339), The Key Clinical Medicine Center of Shanghai (2017ZZ01006), Sanming Project of Medicine in Shenzhen (SZSM201612078), Shanghai Rising-Star Project (18QB1400500) and The Introduction Project of Clinical Medicine Expert Team for Suzhou (SZYJTD201714), Development Project of Shanghai Peak Disciplines-Integrative Medicine (20180101) and Shanghai Committee of Science and Technology (19441901600 and 19441902000).

Disclosure

The authors report no conflicts of interest in this work.

References

1. Sanders TL, Maradit Kremers H, Bryan AJ, et al. Incidence of anterior cruciate ligament tears and reconstruction: a 21-year population-based study. *Am J Sports Med*. 2016;44(6):1502–1507. doi:10.1177/0363546516629944
2. Prentice HA, Lind M, Mouton C, et al. Patient demographic and surgical characteristics in anterior cruciate ligament reconstruction: a description of registries from six countries. *Br J Sports Med*. 2018;52(11):716–722. doi:10.1136/bjsports-2017-098674
3. Chen T, Zhang P, Chen J, Hua Y, Chen S. Long-term outcomes of anterior cruciate ligament reconstruction using either synthetics with remnant preservation or hamstring autografts: a 10-year longitudinal study. *Am J Sports Med*. 2017;45(12):2739–2750. doi:10.1177/0363546517721692
4. Tiefenboeck TM, Thurmaier E, Tiefenboeck MM, et al. Clinical and functional outcome after anterior cruciate ligament reconstruction using the LARS system at a minimum follow-up of 10 years. *Knee*. 2015;22(6):565–568. doi:10.1016/j.knee.2015.06.003
5. Gao S, Tang G, Hua D, et al. Stimuli-responsive bio-based polymeric systems and their applications. *J Mater Chem B*. 2019;7(5):709–729. doi:10.1039/C8TB02491J
6. Bekmurzayeva A, Duncanson WJ, Azevedo HS, Kanayeva D. Surface modification of stainless steel for biomedical applications: revisiting a century-old material. *Mater Sci Eng C Mater Bio Appl*. 2018;93:1073–1089. doi:10.1016/j.msec.2018.08.049
7. Yu X, Tang X, Gohil SV, Laurencin CT. Biomaterials for bone regenerative engineering. *Adv Healthc Mater*. 2015;4(9):1268–1285. doi:10.1002/adhm.201400760
8. Surmenev RA, Surmeneva MA, Ivanova AA. Significance of calcium phosphate coatings for the enhancement of new bone osteogenesis–a review. *Acta Biomater*. 2014;10(2):557–579. doi:10.1016/j.actbio.2013.10.036
9. Barillas L, Cubero-Sesin JM, Vargas-Blanco I. Hydroxyapatite coatings on polymers using a custom low-energy plasma spray system. *IEEE Trans Plasma Sci*. 2018;46(7):2420–2424. doi:10.1109/TPS.2018.2810639
10. Lee JH, Jang HL, Lee KM, Baek HR, Jin K, Noh JH. Cold-spray coating of hydroxyapatite on a three-dimensional polyetheretherketone implant and its biocompatibility evaluated by in vitro and in vivo minipig model. *J Biomed Mater Res B Appl Biomater*. 2017;105(3):647–657. doi:10.1002/jbm.b.33589
11. Wang S, Ge Y, Ai C, et al. Enhance the biocompatibility and osseointegration of polyethylene terephthalate ligament by plasma spraying with hydroxyapatite in vitro and in vivo. *Int J Nanomedicine*. 2018;13:3609–3623. doi:10.2147/IJN.S162466
12. Li JJ, Ebied M, Xu J, Zreiqat H. Current approaches to bone tissue engineering: the interface between biology and engineering. *Adv Healthc Mater*. 2018;7:6. doi:10.1002/adhm.v7.6

13. Ke D, Robertson SF, Dernell WS, Bandyopadhyay A, Bose S. Effects of MgO and SiO2 on plasma-sprayed hydroxyapatite coating: an in vivo study in rat distal femoral defects. *ACS Appl Mater Interfaces*. 2017;9(31):25731–25737. doi:10.1021/acsami.7b05574
14. Ai C, Sheng D, Chen J, et al. Surface modification of vascular endothelial growth factor-loaded silk fibroin to improve biological performance of ultra-high-molecular-weight polyethylene via promoting angiogenesis. *Int J Nanomedicine*. 2017;12:7737–7750. doi:10.2147/IJN.S148845
15. Fukui T, Ii M, Shoji T, et al. Therapeutic effect of local administration of low-dose simvastatin-conjugated gelatin hydrogel for fracture healing. *J Bone Miner Res*. 2012;27(5):1118–1131. doi:10.1002/jbmr.1558
16. Zhang P, Han F, Li Y, et al. Local delivery of controlled-release simvastatin to improve the biocompatibility of polyethylene terephthalate artificial ligaments for reconstruction of the anterior cruciate ligament. *Int J Nanomedicine*. 2016;11:465–478. doi:10.2147/IJN.S95032
17. Ishihara T, Miyazaki M, Notani N, Kanezaki S, Kawano M, Tsumura H. Locally applied simvastatin promotes bone formation in a rat model of spinal fusion. *J Orthop Res*. 2017;35(9):1942–1948. doi:10.1002/jor.23479
18. Gentile P, Nandagiri VK, Daly J, et al. Localised controlled release of simvastatin from porous chitosan–gelatin scaffolds engrafted with simvastatin loaded PLGA-microparticles for bone tissue engineering application. *Mater Sci Eng C*. 2016;59:249–257. doi:10.1016/j.msec.2015.10.014
19. Arcos D, Vallet-Regí M. Bioceramics for drug delivery. *Acta Mater*. 2013;61(3):890–911. doi:10.1016/j.actamat.2012.10.039
20. Croisier F, Jérôme C. Chitosan-based biomaterials for tissue engineering. *Eur Polym J*. 2013;49(4):780–792. doi:10.1016/j.eurpolymj.2012.12.009
21. Selvasudha N, Koumaravelou K. The multifunctional synergistic effect of chitosan on simvastatin loaded nanoparticulate drug delivery system. *Carbohydr Polym*. 2017;163:70–80. doi:10.1016/j.carbpol.2017.01.038
22. Soares DG, Anovazzi G, Bordini EAF, et al. Biological analysis of simvastatin-releasing chitosan scaffold as a cell-free system for pulp-dentin regeneration. *J Endod*. 2018;44(6):971–976 e971. doi:10.1177/0363546517721692
23. Wang X, Schwartz Z, Gittens RA, et al. Role of integrin alpha2 beta1 in mediating osteoblastic differentiation on three-dimensional titanium scaffolds with submicron-scale texture. *J Biomed Mater Res Part A*. 2015;103(6):1907–1918. doi:10.1002/jbm.a.35323
24. Deligianni DD, Katsala ND, Koutsoukos PG, Missirlis YF. Effect of surface roughness of hydroxyapatite on human bone marrow cell adhesion, proliferation, differentiation and detachment strength. *Biomaterials*. 2001;22(1):87–96.
25. Livak KJ, Schmittgen TD. Analysis of relative gene expression data using real-time quantitative PCR and the 2(-Delta Delta C(T)) Method. *Methods*. 2001;25(4):402–408. doi:10.1006/meth.2001.1262
26. Rahman ZU, Shabib I, Haider W. Surface characterization and cytotoxicity analysis of plasma sprayed coatings on titanium alloys. *Mater Sci Eng C Mater Bio Appl*. 2016;67:675–683. doi:10.1016/j.msec.2016.05.070
27. Torstrick FB, Lin ASP, Potter D, et al. Porous PEEK improves the bone-implant interface compared to plasma-sprayed titanium coating on PEEK. *Biomaterials*. 2018;185:106–116. doi:10.1016/j.biomaterials.2018.09.009
28. Pullisaar H, Reseland JE, Haugen HJ, Brinchmann JE, Østrup E. Simvastatin coating of TiO2 scaffold induces osteogenic differentiation of human adipose tissue-derived mesenchymal stem cells. *Biochem Biophys Res Commun*. 2014;447(1):139–144. doi:10.1016/j.bbrc.2014.03.133
29. Yu WL, Sun TW, Qi C, et al. Enhanced osteogenesis and angiogenesis by mesoporous hydroxyapatite microspheres-derived simvastatin sustained release system for superior bone regeneration. *Sci Rep*. 2017;7:44129. doi:10.1038/srep44129
30. Iwamoto T, Hieda Y, Kogai Y. Effect of hydroxyapatite surface morphology on cell adhesion. *Mater Sci Eng C*. 2016;69:1263–1267. doi:10.1016/j.msec.2016.07.056
31. Costa DO, Prowse PDH, Chrones T, et al. The differential regulation of osteoblast and osteoclast activity by surface topography of hydroxyapatite coatings. *Biomaterials*. 2013;34(30):7215–7226. doi:10.1016/j.biomaterials.2013.06.014
32. Ai-Aql ZS, Alagl AS, Graves DT, Gerstenfeld LC, Einhorn TA. Molecular mechanisms controlling bone formation during fracture healing and distraction osteogenesis. *J Dent Res*. 2008;87(2):107–118. doi:10.1177/154405910808700215
33. Bobbert F, Zadpoor A. Effects of bone substitute architecture and surface properties on cell response, angiogenesis, and structure of new bone. *J Mater Chem B*. 2017;5(31):6175–6192. doi:10.1039/C7TB00741H
34. Pullisaar H, Tiainen H, Landin MA, et al. Enhanced in vitro osteoblast differentiation on TiO2 scaffold coated with alginate hydrogel containing simvastatin. *J Tissue Eng*. 2013;4:2041731413515670. doi:10.1177/2041731413515670
35. Martin JY, Schwartz Z, Hummert TW, et al. Effect of titanium surface roughness on proliferation, differentiation, and protein synthesis of human osteoblast-like cells (MG63). *J Biomed Mater Res*. 1995;29(3):389–401. doi:10.1002/jbm.820290314
36. Finelle G, Papadimitriou DEV, Souza AB, Katebi N, Gallucci GO, Araújo MG. Peri-implant soft tissue and marginal bone adaptation on implant with non-matching healing abutments: micro-CT analysis. *Clin Oral Implants Res*. 2014;26(4):e42–e46. doi:10.1111/clr.12328
37. Cai J, Wan F, Dong Q, et al. Silk fibroin and hydroxyapatite segmented coating enhances graft ligamentization and osseointegration processes of the polyethylene terephthalate artificial ligament in vitro and in vivo. *J Mater Chem B*. 2018;6(36):5738–5749. doi:10.1039/C8TB01310A
38. Kim HD, Amirthalingam S, Kim SL, Lee SS, Rangasamy J, Hwang NS. Biomimetic materials and fabrication approaches for bone tissue engineering. *Adv Healthc Mater*. 2017;6:23.
39. Oka S, Matsumoto T, Kubo S, et al. Local administration of low-dose simvastatin-conjugated gelatin hydrogel for tendon-bone healing in anterior cruciate ligament reconstruction. *Tissue Eng Part A*. 2013;19(9–10):1233–1243. doi:10.1089/ten.TEA.2012.0325
40. Muzzarelli RAA. Chitosan composites with inorganics, morphogenetic proteins and stem cells, for bone regeneration. *Carbohydr Polym*. 2011;83(4):1433–1445. doi:10.1016/j.carbpol.2010.10.044